Low-Impedance VHF and UHF Capacitive Silicon Bulk Acoustic Wave Resonators—Part I: Concept and Fabrication

Siavash Pourkamali, *Member, IEEE*, Gavin K. Ho, *Student Member, IEEE*, and Farrokh Ayazi, *Senior Member, IEEE*

***Abstract*—This paper presents high-performance high-frequency single-crystal silicon (SCS) capacitive resonators. Long and thick bulk-micromachined resonating block structures, which are referred to as "silicon bulk acoustic wave resonator" (SiBAR), are fabricated using the high-aspect-ratio poly and single crystalline silicon" (HARPSS) fabrication process on silicon-on-insulator (SOI) substrates. Such resonators operate in their horizontal width extensional modes with quality factors in the range of 10 000–100 000. With their comparatively large electrode area and deep-submicrometer capacitive transduction gaps, such resonators have demonstrated comparatively low impedances for capacitive resonators that are well within the desired range for high-frequency electronic applications. Sub-kilo-Ohm total electrical resistances and extracted motional resistance as low as 200 Ω are demonstrated for the fundamental width extensional modes of SiBARs in the very-high-frequency range. Resonant frequencies up to 1.55 GHz are demonstrated for the higher resonance modes of the capacitive SiBARs with comparatively low impedances. Part I of this paper presents the basic operation concepts and fabrication methodology for the HARPSS-on-SOI SiBARs. Extensive resonator measurement data, including temperature characteristics, are presented in Part II of this paper, and different frequency tuning approaches for temperature compensation of such resonators are discussed and investigated.**

***Index Terms*—Bulk acoustic wave resonators, high-aspect-ratio poly and single crystalline silicon (HARPSS), MEMS, micromachining, micromechanical resonators, silicon resonators.**

I. Introduction

A VARIETY OF high-frequency micromechanical resonator technologies are currently under investigation, targeting realization of viable and more efficient replacements for the existing technologies such as quartz [1], surface acoustic wave [2]–[4], and film bulk acoustic wave resonators (FBARs) [5], [6]. Resonators and filters that are implemented using such technologies have a wide range of applications in electronics as highly stable frequency references and bandpass filters (e.g., radio frequency front-end duplexer filters), as well as chemical and biomedical gravimetric sensors [4], [6]. Among the most successful newly developed technologies are miniaturized quartz resonators [7], piezoelectric in plane resonators [8], [9], and capacitive (electrostatic) silicon resonators [10]–[21].

Capacitive resonators can be fully made of IC-compatible materials such as silicon and silicon dioxide and can be embedded in a variety of IC technologies, resulting in higher levels of integration, and cost savings. The availability of well-established and low-cost nanoprecision batch-fabrication processes developed for IC manufacturing is another motivating factor for the implementation of silicon-based capacitive resonators.

Other advantages of capacitive silicon resonators from the system design point of view are as follows: 1) the resonance frequency of capacitive resonators can be slightly tuned by changing the dc bias voltage that is required for their operation; such tunability can be used for postfabrication fine tuning or temperature compensation of the resonators [16], [17] and 2) the modulation effect provided by the polarization voltage for capacitive resonators can be used to turn them into narrowband mixers [18] or turn them on and off when needed.

On the other hand, while impedances in the 50-Ω range are easily achievable for the piezoelectric resonators, typical capacitive resonators with frequencies in the very high frequency (VHF) and ultra-high frequency (UHF) range have impedances on the order of tens or hundreds of kiloohms [10]–[14]. The reason for much larger impedance of capacitive resonators is the nature of electrostatic transduction mechanism and its actuation forces, which are generally much smaller (i.e., two to three orders of magnitude) than piezoelectric forces that are generated under similar conditions. Despite utilization of several fabrication and mechanical design techniques [11]–[14], [19], [20] to alleviate the impedance issue for air gap capacitive resonators, the demonstrated impedances in the VHF and UHF range are not promising yet. The alternative category of electrostatic resonators that have been under investigation during the past few years is dielectric gap electrostatic resonators [21], [22], in which the electrostatic transduction forces are generated using a high-k dielectric material instead of air in the electrostatic actuation gap. As a result, larger forces can be generated, resulting in lower resonator impedances. Although promising results have been demonstrated using this approach, such devices suffer from large electrode-resonator capacitances, as well as lower quality factors compared to air gap resonators and material mismatch and characterization issues.

Manuscript received October 11, 2006; revised March 29, 2007. The review of this paper was arranged by Editor K. Najafi.

S. Pourkamali is with the Department of Electrical and Computer Engineering, University of Denver, Denver, CO 80208 USA.

G. K. Ho and F. Ayazi are with the School of Electrical and Computer Engineering, Georgia Institute of Technology, Atlanta, GA 30332-0250 USA (e-mail: ayazi@ece.gatech.edu).

Color versions of one or more of the figures in this paper are available online at http://ieeexplore.ieee.org.

Digital Object Identifier 10.1109/TED.2007.901403

The concept of silicon bulk acoustic wave resonators (SiBARs) and preliminary fabrication and characterization results for such devices was initially presented in [15]. It was shown that due to their much larger transduction area, SiBARs can provide significantly lower motional resistances compared to the previously demonstrated disk resonators [10], [13], [14] while maintaining the same high-quality factors. In [15], close to one order of magnitude lower impedances were demonstrated for the SiBARs operating in the VHF band. In this paper, extensive measurement and characterization data for SiBARs with several dimensions are presented. It is practically shown that having quarter-wavelength-long support beams for clamped–clamped SiBARs does not have a significant effect on the Q of such resonators. Therefore, the new SiBAR structures in this paper have short and stiff support beams that make them capable of tolerating much larger polarization voltages without getting pulled in. As a result, another order of magnitude reduction in the equivalent electrical impedances and values well within the desired range for electronic applications are demonstrated for VHF SiBARs. This makes high-aspect-ratio poly and single crystalline silicon (HARPSS) capacitive SCS resonators a very strong candidate for implementation of silicon-based low-phase-noise tunable integrated frequency references. In addition, some of the lowest impedances reported to date for air gap capacitive resonators in the gigahertz frequency range ($\sim$10$\times$ lower than those in [10]–[12]) are demonstrated for the higher resonance modes of the SiBAR structures. SiBARs and other HARPSS-based capacitive resonators operate in their horizontal (in-plane) resonance modes for which the resonance frequencies are determined by their lithographically defined dimensions. Therefore, resonators with a wide range of frequencies (tens of kilohertz up to a few gigahertz) can be fabricated simultaneously on a single substrate. Such flexibility is not available in most of the traditional piezoelectric resonator and FBAR technologies.

As highly stable frequency references, temperature behavior and compensation techniques for high-frequency capacitive SiBARs are of great importance. A large tuning range can be achieved by changing the temperature of the high-frequency SiBARs. Accordingly, an active self-compensating strategy that is based on simultaneous usage of the resonator itself as a heater and a temperature sensor is discussed, and its feasibility for SiBARs is investigated.

II. Device Concept and Operation

For rectangular block resonators presented in this paper, the horizontal dimension, which is called the "width," determines the frequency of the bulk extensional resonance mode. Therefore, unlike the disk resonators, a high operating frequency can be maintained while extending the other horizontal dimension (i.e., the length) to provide a large transduction area and, consequently, lower its equivalent electrical impedance. Using the HARPSS fabrication technology, while increasing the resonator length, one can extend the resonator thickness in the vertical direction as well [13]–[15] to achieve tens to hundreds of times larger transduction area compared to the surface-micromachined disk resonators [10]. Such structure will be a standing plate that resonates in its bulk mode similar to FBARs. Fig. 1 shows the schematic view of a piezoelectric FBAR [Fig. 1(a)], as well as a vertically placed silicon version of the same structure. The bare silicon resonating membrane [Fig. 1(b)] is placed in between two electrodes that are separated from the resonator by narrow capacitive gaps to operate the resonator electrostatically in its horizontal width extensional mode [Fig. 1(b)]. In this paper, such a resonator is referred to as a SiBAR.

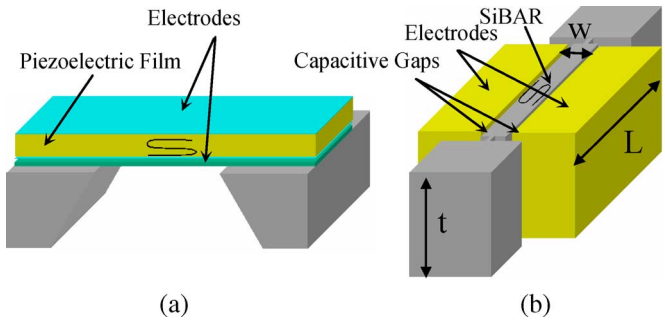

Fig. 1. Schematic diagram of (a) a piezoelectric FBAR and (b) a vertical capacitive SiBAR.

As opposed to the FBARs for which the resonant frequency is determined by the thickness of a deposited piezoelectric film, the resonant frequency of the SiBARs is determined by their lithography-defined horizontal width. Therefore, SiBARs with different resonant frequencies can be simultaneously fabricated on the same substrates.

A. Fundamental Width-Extensional Mode

Fig. 2 presents the ANSYS modal analysis results that show the fundamental width-extensional mode shapes for a 160-μm-long 40-μm-wide SiBAR with different thicknesses. Fig. 2 clearly shows that as the resonator thickness increases to values that are close to its width and higher, the mode shape of the width extensional mode becomes distorted, showing a wavy nonuniform pattern. This may result in partial cancellation of the electromechanical coupling between the resonator and electrodes and, consequently, higher equivalent impedances. Therefore, precautions need to be taken in designing thick SiBARs to avoid excessive cancellation for the desired mode. Such wavy patterns are observed in FBARs as well [23]. However, due to a much larger electromechanical coupling coefficient for the piezoelectric transducers, the coupling degradation caused by the distorted mode shape can be tolerated in FBARs.

The other trend that can be observed in Fig. 2 is that a sharp shift in the resonance frequency is observed for the distorted mode shapes, whereas for thin resonators with a uniform thickness, the resonance frequency does not have a significant dependence on the resonator thickness. Prediction and analysis of thickness-induced frequency shifts is out of the scope of this paper; however, the observed trend in Fig. 2 suggests that the frequency decreases as the resonator thickness gets close to its width and goes back up to even higher values for larger thicknesses. This can be explained by the distorted nature of the mode shapes that can change to a totally different shape with slight changes in the thickness. Therefore, for realization

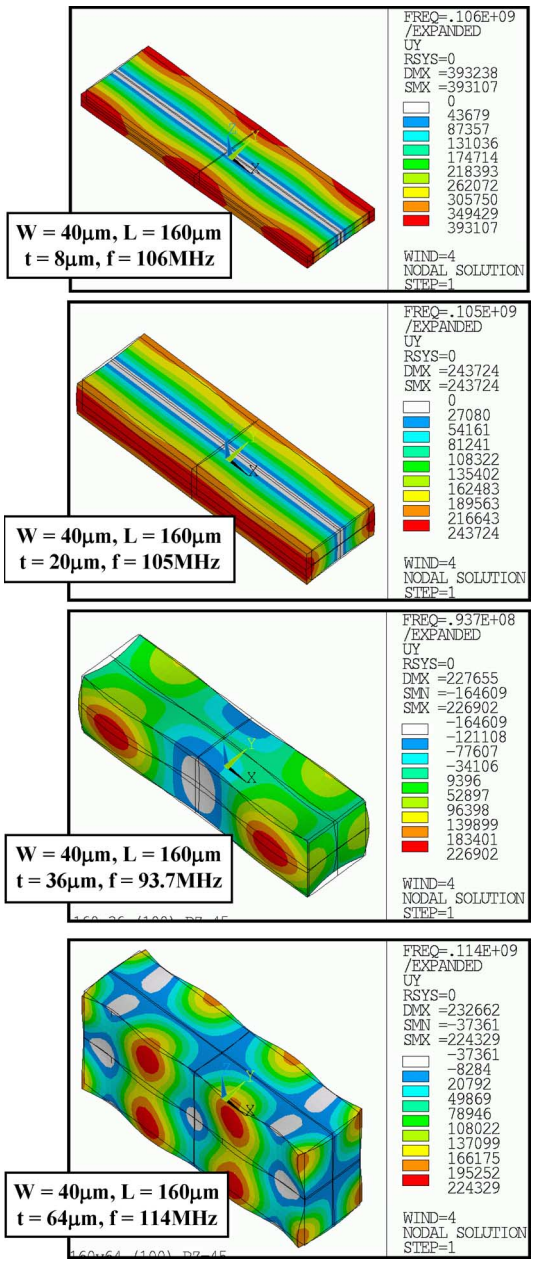

Fig. 2. ANSYS modal analysis, showing the width extensional mode shape for a 160-μm-long 40-μm-wide SiBAR with a thickness that ranges from 8 to 64 μm, showing how the mode shape becomes distorted as the resonator thickness increases.

of high-precision frequency references, in addition to precise control of the dimensions, one has to consider such higher order effects when choosing the resonator dimensions so that it can tolerate slight dimension changes while keeping its resonant frequency in the desired range.

Equation (1) gives the electrical equivalent resistance for a generic two-port in-plane capacitive block resonator

$$R_m = \frac{\gamma\sqrt{KM}g^4}{Q\varepsilon_0^2 L_e^2 t^2 V_p^2} \propto \frac{\gamma g^4}{Q \cdot V_p^2 \cdot L_e \cdot t} \tag{1}$$

where K and M are the effective mechanical mass and stiffness of the resonator, g is the capacitive gap size, Q is the quality factor of the resonator, V_p is the applied dc polarization voltage, L_e is the physical electrode length, t is the thickness (height) of the structure, and γ, which is referred to as the "coupling ratio," is a coefficient that indicates how effective the electromechanical coupling between the resonator and the electrodes is. The value of γ varies from 1, for a completely uniform mode shape with flat resonator sidewalls, to 0, for a wavy mode shape with complete charge cancellation.

Equation (2) gives the resonance frequency for a thin and narrow block resonator (bar), assuming that the poisson's ratio is zero [24]

$$f_n = \frac{n}{2W} \cdot \sqrt{\frac{E}{\rho}} \tag{2}$$

where n is the width extensional mode number, which is an integer (i.e., $n = 1, 2, \ldots$), W is the width (frequency-determining dimension) of the block, and E and ρ are the Young's modulus and density of the structural material, respectively. SiBARs are long and thick block resonators that operate in a similar resonance mode; therefore, the same equation can be used to calculate the resonance frequency of SiBARs with good approximation. To determine the exact resonance frequency for SiBARs, finite-element modal analysis needs to be performed for each specific set of dimensions.

The effective mass for each resonance mode can be calculated by integrating the square of the normalized vibration amplitude over the volume of the structure [24]. Since the mode shape for the extensional mode of a bar is a sinusoidal function [24], the effective mass for the extensional mode is half the static mass of the resonator, i.e., $M = \rho \cdot L \cdot W \cdot t/2$. The effective stiffness can then be calculated based on the effective mass and resonance frequency ($K = M\omega^2$).

The gap size, g, has the most significant effect on the equivalent resistance of the capacitive resonators. However, excessive reduction of the gap size will eventually result in nonlinearity, and limit the dynamic range of the device. In addition, the maximum applicable bias voltage reduces by decreasing the gap size and partially cancels the effect of gap size reduction on the electrical impedance of the resonator. Increasing the thickness of the resonators to decrease the equivalent resistance was demonstrated for HARPSS VHF disk resonators [13], [14]. It was theoretically shown that impedances in the subkilo-ohm range can be achieved for disk resonators in the VHF (30–300 MHz) range by aggressively pushing the fabrication limits to produce larger thicknesses and smaller capacitive gaps. However, for UHF (300 MHz to 3 GHz) disk resonators with diameters smaller than 10 μm, the available area for sensing and actuation is extremely limited, resulting in even higher impedances. The alternative option is to use higher resonance modes of larger disk resonators [10]; however, higher resonance modes also have higher mechanical equivalent stiffness, and therefore in any case, for disk resonators, the impedance will increase by increasing the resonance frequency. SiBARs that are fabricated using the HARPSS process can be a few to a few tens of micrometers thick and tens to thousands of micrometers long, providing a much larger capacitive transduction area. This sets the platform for implementation of low-impedance VHF

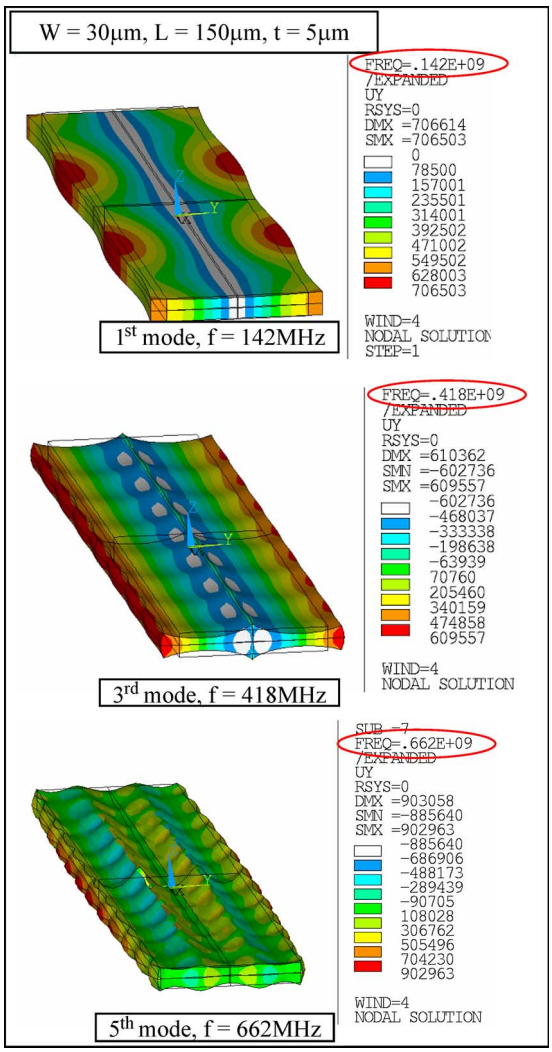

Fig. 3. ANSYS modal analysis, showing the mode shapes for the first, third and fifth width extensional modes of a SiBAR structure.

and UHF air gap capacitive resonators without the need for aggressive reduction of the capacitive gap sizes.

B. Higher Width-Extensional Modes

Similar to the beam [25] or disk [10] resonators, SiBARs can also be operated in their higher width-extensional resonance modes. Fig. 3 shows ANSYS modal analysis results for a thin SiBAR structure, showing the mode shapes for its first, third, and fifth width-extensional modes.

A similar argument about the effect of resonator thickness on its mode shape applies to the higher modes of SiBARs. Clean and uniform mode shapes with a large coupling ratio can be obtained when the resonator thickness is smaller than its effective width. For higher modes, the effective width is n times smaller than the physical width of the resonator, where n is the mode number. For the fifth resonant mode of the 30-μm-wide SiBAR of Fig. 3, the effective width is $30/5 = 6$ μm, which is close to its thickness (5 μm), and therefore, severe distortion of the mode shape can be clearly observed for the fifth resonance mode.

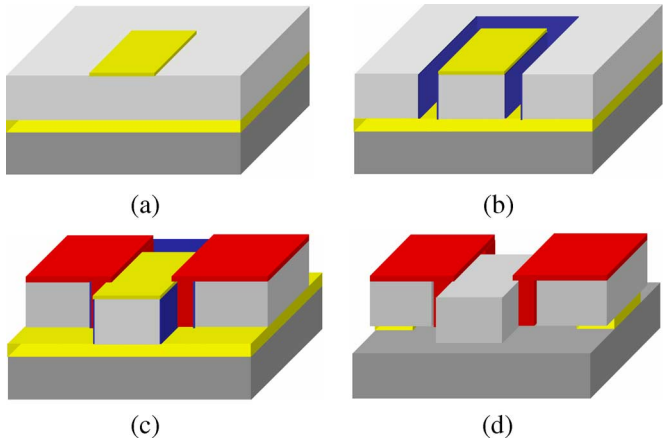

Fig. 4. Process flow of the three-mask HARPSS-on-SOI approach used for the fabrication of thick SCS bulk mode resonators. (a) Grow and pattern initial oxide. (b) Etch trenches, deposit LPCVD sacrificial oxide etch back oxide. (c) Pattern silicon substrate and polysilicon inside the trenches. (d) HF release.

The motional resistance for the nth width extensional mode of a SiBAR, assuming a nondistorted mode shape, is n times larger than that of a SiBAR with the same dimensions that operate in its first mode. This can be explained using (1), where the electrode dimensions are the same for the two resonators but the effective stiffness is n^2 times larger for the higher resonance mode, resulting in an impedance that is n times larger.

III. Resonator Fabrication: HARPSS-on-SOI

Several varieties of HARPSS-based fabrication processes have been used for the implementation of micromechanical resonators on both regular silicon [25] and SOI substrates [13]–[15]. The latest version of the HARPSS-on-SOI process, which can be performed with as low as three lithography steps [14], [15], was used in this paper for the fabrication of thick single-crystal SiBARs with polysilicon sense and drive electrodes. Electrodes are separated from the resonators with deep-submicrometer (100–250 nm) capacitive gaps. The major advantage of HARPSS-based fabrication processes is their ability to implement ultra-high-aspect-ratio capacitive gaps (as high as 460, as demonstrated in this paper) between polysilicon and SCS structures that are tens of micrometers thick. HARPSS gap aspect ratios can easily be up to 10$\times$ larger than the largest achievable aspect ratios using the state-of-the-art deep reactive-ion etching tools.

The process flow is shown in Fig. 4 and consists of only three lithography steps and a number of thin-film deposition and etching steps. The process starts with thermally growing a comparatively thick oxide layer (0.5–1.5 μm thick) on the low-resistivity SOI substrate. The oxide is patterned and kept only on top of the body of the resonators, as well as the polarization voltage wirebonding pads that are physically connected to the resonators [Fig. 4(a)]. This oxide layer acts as a mask to protect the structures against the silicon-etching plasma during the following silicon and polysilicon etch steps. Vertical trenches are then etched around the resonators using the Bosch process all the way down to the SOI buried oxide to define the shape of the resonator in the SOI device layer. The thickness of the

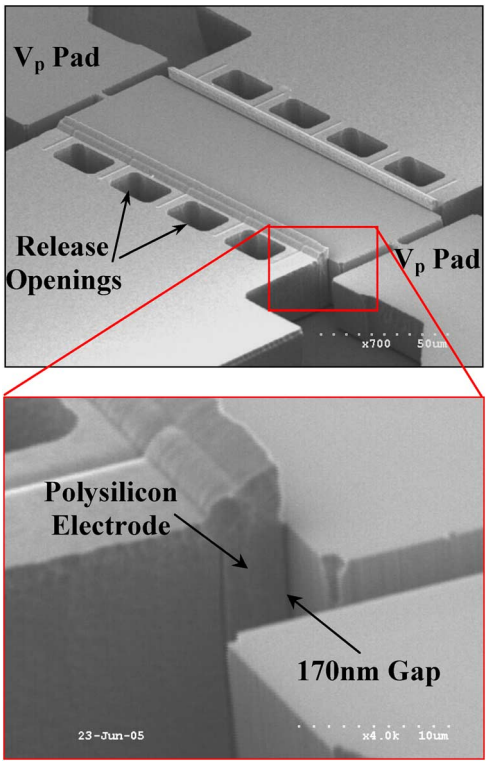

Fig. 5. SEM view of a 50-μm-wide 150-μm-long 20-μm-thick SiBAR and close-up of its electrode, showing the 170-nm capacitive gap.

resonators is determined by the SOI device layer thickness and can be as large as a few tens of micrometers. A thin layer of sacrificial oxide is then deposited using low-pressure chemical vapor deposition (LPCVD) or thermally grown, which uniformly covers all the silicon surfaces, including the trench sidewalls. The thickness of the sacrificial oxide layer determines the capacitive gap size in between the SCS resonators and their polysilicon electrodes and can be as small as a few tens of nanometers. The sacrificial oxide is etched back on the surface [Fig. 4(b)] so that the polysilicon pads for the electrodes will be directly connected to the silicon and stay firmly anchored during the hydrofluoric acid (HF) release at the end of the process.

Trenches are subsequently refilled with highly p-type doped polysilicon that forms the electrodes. The silicon device layer is patterned to provide electrical isolation between different devices, as well as the input, output, and body of individual resonators. At the same time, the polysilicon inside the trenches is patterned and kept only in the electrode area [Fig. 4(c)]. Structures are finally released and undercut in HF by removing the sacrificial oxide layer and the underlying buried oxide [Fig. 4(d)].

Single-crystal SiBARs with different thickness (5–30 μm) and capacitive gap sizes (65–225 nm) and operating frequencies in the VHF and UHF range were fabricated using the described processing technique.

Fig. 5 is the SEM view of a fabricated 20-μm-thick 50-μm-wide 150-μm-long SiBAR, as well as the close-up of its 170-nm capacitive gap. The resonator is supported on the two sides by tiny support beams. Support beams are placed in

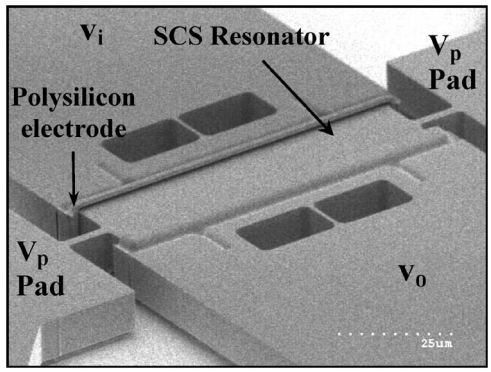

Fig. 6. SEM view of a 20-μm-wide 80-μm-long 10-μm-thick SiBAR and close-up of the support area and 225-nm capacitive gap of the same resonator. Electrodes cover the edges of the SiBAR.

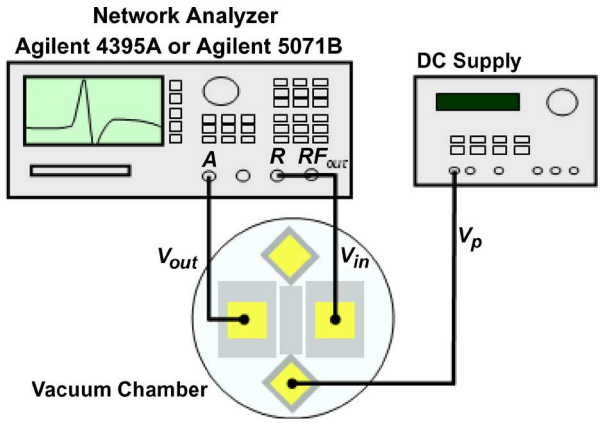

Fig. 7. Schematic diagram of the test setup used for resonator measurement and characterization.

the midpoint of the resonator width, which has a zero vibration amplitude along the width to minimize the loss of energy from the resonating body to the substrate. The rectangular openings in the electrode pads are etched during the last lithography and etching step to facilitate and accelerate resonator undercutting in HF.

Fig. 6 shows a fabricated 10-μm-thick 20-μm-wide 80-μm-long clamped–clamped SiBAR. The resonator has 225-nm capacitive gaps and is supported on the two sides by 3-μm-wide 10-μm-long support beams. In addition to placing the support beams in the midpoint of the resonator width, the length of the supports is chosen to be equal to the quarter acoustic wavelength at the operating frequency (half of the bulk acoustic wave resonator width) to further minimize the flow of energy to the substrate and maximize the quality factor of the resonator.

IV. Resonator Measurement

The test setup that is shown in Fig. 7 was used for characterization of the fabricated resonators. In this approach, the silicon chip that contains a number of resonators is mounted on a simple printed circuit board (PCB) with coaxial connectors. The resonator input, output, and polarization voltage pads are then wire-bonded to the copper traces on the PCB that are connected to the coaxial connectors, and the connectors are connected

to the network analyzer, as well as a dc bias source using coaxial cables. Therefore, the resonators are directly connected to the network analyzer without any buffer or amplifier in between.

For characterization in vacuum, the PCB is placed inside a custom-made vacuum chamber with coaxial feedthroughs.

To cancel the effect of the parasitics associated with the PCB and cables, a response and isolation calibration is performed on the network analyzer with the resonator connected in its "OFF" state (i.e., V_p set to zero). In this manner, the effect of the resonator feedthrough and pad capacitances, as well as any other parasitic associated with the PCB and wire-bonds is cancelled out, and a clear resonance peak can be observed after the resonator is turned on. The quality factor of each resonance mode is then calculated by the network analyzer based on its associated resonance peak. The quality factor measured by the network analyzer is affected by any series resistance in the resonator path, including termination resistors, as well as any other resistances in the silicon structure of the resonator (3). That is

$$Q_{\rm res} \propto \frac{1}{R_{\rm res}}, \quad \text{and} \quad Q_{\rm measured} \propto \frac{1}{R_{\rm load}+R_m} \Rightarrow \frac{Q_{\rm res}}{Q_{\rm measured}} = \frac{R_{\rm load}+R_m}{R_m} \quad (3)$$

where $Q_{\rm res}$ is the intrinsic mechanical Q of the resonator, $R_{\rm load}$ is the parasitic series resistance that loads the Q of the resonator, and R_m is the motional resistance of the resonator.

At its resonant frequency, the resonator is equivalent to an electrical resistance that is terminated by two parallel capacitors to ground, which are cancelled out by calibration. When directly connected to the 50-Ω terminations of the network analyzer, the value of the equivalent motional resistance of the resonators can be extracted from the frequency response plots using the following equation:

$$R_{\rm eq} = 50 \times 10^{\frac{Atn.}{20}} \quad (4)$$

where $Atn.$ is the measured attenuation (in decibels) at the resonance peak.

Extensive measurement results for the fabricated resonators are presented in Part II of this paper.

REFERENCES

[1] M. E. Frerking, "Fifty years of progress in quartz frequency standards," in *Proc. IEEE Int. Freq. Control Symp.*, 1996, pp. 33–46.

[2] P. V. Wright, "A review of SAW resonator filter technology," in *Proc. IEEE Ultrason. Symp.*, 1992, pp. 29–38.

[3] M. Ueda *et al.*, "Ultra-miniaturized and high performance PCS SAW duplexer with steep cut-off filters," in *Proc. MTT-S*, 2004, vol. 2, pp. 913–916.

[4] E. Berkenpas, S. Bitla, P. Millard, and M. P. da Cunha, "Pure shear horizontal SAW biosensor on langasite," *IEEE Trans. Ultrason., Ferroelectr., Freq. Control*, vol. 51, no. 11, pp. 1404–1411, Nov. 2004.

[5] R. C. Ruby *et al.*, "Thin film bulk wave acoustic resonators (FBAR) for wireless applications," in *Proc. Ultrason. Symp.*, 2001, pp. 813–821, vol. 1.

[6] A. Dickherber, C. D. Corso, and W. Hunt, "Lateral field excitation (LFE) of thickness shear mode (TSM) acoustic waves in thin film bulk acoustic resonators (FBAR) as a potential biosensor," in *Proc. 28th IEEE Int. Conf. EMBS*, 2006, pp. 4590–4593.

[7] D. T. Chang *et al.*, "A new MEMS-based quartz resonator technology," in *Proc. Hilton Head*, 2004, pp. 41–44.

[8] S. Humad, R. Abdolvand, G. K. Ho, and F. Ayazi, "High frequency micromechanical piezo-on-silicon block resonators," in *IEDM Tech. Dig.*, 2003, pp. 957–960.

[9] G. Piazza and A. P. Pisano, "Dry-released post-CMOS compatible contour-mode aluminum nitride micromechanical resonators for VHF applications," in *Proc. Hilton Head*, 2004, pp. 37–40.

[10] J. Wang, Z. Ren, and C. T.-C. Nguyen, "Self-aligned 1.14 GHz vibrating radial-mode disk resonators," in *Proc. Transducers*, 2003, pp. 947–950.

[11] S. Li *et al.*, "Micromechanical hollow disk ring resonators," in *Proc. MEMS*, 2004, pp. 821–824.

[12] E. P. Quévy *et al.*, "Poly-SiGe high frequency resonators based on lithographic definition of nano-gap lateral transducers," in *Proc. Solid-State Sens., Actuators, Microsyst. Workshop (Hilton Head)*, 2004, pp. 360–363.

[13] S. Pourkamali *et al.*, "VHF single crystal silicon capacitive elliptic bulk-mode disk resonators—Part II: Implementation and characterization," *J. Microelectromech. Syst.*, vol. 13, no. 6, pp. 1054–1062, Dec. 2004.

[14] S. Pourkamali and F. Ayazi, "High frequency capacitive micromechanical resonators with reduced motional resistance using the HARPSS technology," in *Proc. 5th Silicon RF Top. Meeting*, 2004, pp. 147–150.

[15] S. Pourkamali, G. K. Ho, and F. Ayazi, "Vertical capacitive SiBARs," in *Proc. MEMS*, 2005, pp. 211–214.

[16] G. K. Ho *et al.*, "Low impedance, highly tunable, I2-resonators for temperature compensated reference oscillators," in *Proc. MEMS*, 2005, pp. 116–120.

[17] G. K. Ho *et al.*, "Temperature compensated IBAR reference oscillators," in *Proc. MEMS*, 2006, pp. 910–913.

[18] A.-C. Wong and C. T.-C. Nguyen, "Micromechanical mixer-filters ("mixlers")," *J. Microelectromech. Syst.*, vol. 13, no. 1, pp. 100–112, Feb. 2004.

[19] M. U. Demirci and C. T.-C. Nguyen, "Mechanically corner-coupled square microresonator array for reduced series motional resistance," *J. Microelectromech. Syst.*, vol. 15, no. 6, pp. 1419–1436, Dec. 2006.

[20] S. Lee and C. T.-C. Nguyen, "Mechanically-coupled micromechanical arrays for improved phase noise," in *Proc. IEEE Int. Ultrason., Ferroelectr., Freq. Control 50th Anniv. Joint Conf.*, Montreal, PQ, Canada, Aug. 24–27, 2004, pp. 280–286.

[21] H. Chandrahalim, D. Weinstein, L. F. Cheow, and S. A. Bhave, "Channel-select micromechanical filters using high-K dielectrically transduced MEMS resonators," in *Proc. MEMS*, Jan. 2006, pp. 894–897.

[22] S. A. Bhave and R. T. Howe, "Silicon nitride-on-silicon bar resonator using internal electrostatic transduction," in *Proc. Transducers*, 2005, pp. 2139–2142.

[23] A. S. Paulo *et al.*, "Atomic force microscopy characterization of electromechanical properties of RF acoustic bulk wave resonators," in *Proc. MEMS*, 2004, pp. 169–172.

[24] J. H. Ginsberg, *Mechanical and Structural Vibrations*. Hoboken, NJ: Wiley, 2001.

[25] S. Pourkamali *et al.*, "High-Q single crystal silicon HARPSS capacitive beam resonators with self-aligned sub-100 nm transduction gaps," *J. Microelectromech. Syst.*, vol. 12, no. 4, pp. 487–496, Aug. 2003.

Siavash Pourkamali (S'02–M'06) received the B.S. degree in electrical engineering from Sharif University of Technology, Tehran, Iran, in 2001 and the M.S. and Ph.D. degrees from Georgia Institute of Technology, Atlanta, in 2004 and 2006, respectively.

He is currently an Assistant Professor in the Department of Electrical and Computer Engineering, University of Denver, Denver, CO. He is the holder of five patents in the areas of silicon micro/nanomechanical resonators and filters, and nanofabrication technologies. His main research interests are integrated silicon MEMS and microsystems, micromachining technologies, RF MEMS resonators and filters, nanomechanical resonant sensors, and micro/nanorobotics for cell and molecular biology.

Prof. Pourkamali was the recipient of the 2005 Georgia Tech Sigma Xi Best M.S. Thesis Award, a 2006 Georgia Tech Electrical and Computer Engineering Research Excellence Award, and a silver medal in the 29th International Chemistry Olympiad.

Gavin K. Ho (S'01) was born in Vancouver, BC, Canada. He received the M.Eng. and B.A.Sc. degrees [with distinction in mechanical engineering (electromechanical design option)] from the University of British Columbia, Canada in 2001. He is currently working toward the Ph.D. degree in the School of Electrical and Computer Engineering, Georgia Institute of Technology (Georgia Tech), Atlanta.

He then joined Georgia Tech, where he was given the opportunity to teach undergraduate courses. His primary teaching objectives include instilling curiosity in science and motivating interdisciplinary research. His research interests include capacitive and piezoelectric micromechanical resonators for sensors, reference oscillators, and bandpass filter applications.

Mr. Ho was the recipient of the UBC Letson Prize in 2001 and the Col. Oscar P. Cleaver Award and N. Walter Cox Fellowship from the School of Electrical and Computer Engineering, Georgia Tech.

Farrokh Ayazi (S'96–M'00–SM'05) received the B.S. degree from the University of Tehran, Tehran, Iran, in 1994 and the M.S. and Ph.D. degrees from the University of Michigan, Ann Arbor, in 1997 and 2000, respectively, all in electrical engineering.

He joined the faculty of Georgia Institute of Technology, Atlanta, in December 1999, where he is currently an Associate Professor in the School of Electrical and Computer Engineering. His research interests are integrated micro- and nanoelectromechanical resonators, IC design for MEMS and sensors, RF MEMS, inertial sensors, and microfabrication techniques.

Prof. Ayazi was the recipient of the National Science Foundation CAREER Award in 2004, the Richard M. Bass Outstanding Teacher Award (determined by the vote of the ECE senior class) in 2004, the Georgia Tech College of Engineering Cutting Edge Research Award for 2001–2002, and a Rackham Predoctoral Fellowship from the University of Michigan for 1998–1999. He is an Editor for the IEEE/ASME JOURNAL OF MICROELECTROMECHANICAL SYSTEMS and serves on the technical program committees of the IEEE International Solid-State Circuits Conference and the International Conference on Solid-State Sensors, Actuators and Microsystems (Transducers).